Nonlinear Control for Maneuvering Multiple Flexible Mode Systems

Chanat La-orpacharapan and Lucy Y. Pao

Abstract— **This paper derives closed-loop control laws using a phase-plane approach for flexible structures having two flexible modes. The flexible modes are addressed by using multi-mode input shapers to shape the time-optimal control for the rigid body portion of the system, and then the altered rigid body phase-plane trajectories resulting from this shaping are solved and used to determine a closed-loop controller. Both "convolution" and "simultaneous" method multi-mode input shapers are considered. Simulations show that the derived control laws applied to a disk drive system yield near time-optimal performance without unwanted residual vibrations.**

I. Introduction

In many applications, to achieve fast response to set-point changes, the moving part is made of lighter material. However, this can lead to flexible dynamics that are difficult to regulate or suppress [1], [3].

While proximate time-optimal servomechanisms (PTOS) and extended PTOS (XPTOS) have been used successfully in many flexible servo systems [2], [8]-[10], [15], these techniques take into account the flexible dynamics of the systems only when the closed-loop systems approach the final settling point. When the flexible dynamics of systems become more significant the control laws need to address the flexible dynamics for the entire slewing motion.

We recently developed a feedback phase-plane control approach called shaped time-optimal servomechanism (STOS) control [4]-[7], [11]. The basic idea of this approach is to address the rigid body and the flexible body separately. It starts off with the time-optimal control command that drives the rigid body portion of the system from rest to rest. Applying this control command to the system would yield vibrations. To address the flexible modes, input shaping [13] is used to alter the phase-plane trajectory due to the time-optimal control profiles. By following these shaped phase-plane trajectories, the derived STOS control drives the closed-loop system from rest to rest in near time-optimal performance with no vibration at the end of the maneuver.

In [11], we derived the STOS control laws for systems consisting of a pure rigid body and one flexible mode with extensions to account for damping in the flexible mode, different acceleration and deceleration rates, and maximum velocity limits. We have also extended the STOS approach for different types of rigid body dynamics. For example, in disk drive systems, taking into account the effect of back electromotive force (EMF) leads to systems having a second-order rigid body with damping and taking into account the effects of back EMF as well as coil inductance leads to systems having a third-order rigid body [4]-[6]. For systems consisting of a pure rigid body or a second-order rigid body with damping, the STOS control laws can be derived analytically in closed form, whereas the STOS control laws for systems with a third-order rigid body have to be numerically derived.

In this paper, we further extend the STOS approach to address systems having multiple flexible modes. Input shaping for multiple flexible modes can be derived by several methods [12], [14]. STOS control laws using both the "convolution" and "simultaneous" method shapers for systems having a pure rigid body with two flexible modes are detailed in Section II. For systems having more than two flexible modes, the STOS control can be derived using a similar procedure as detailed in this paper [7]. Discussion and simulation results of the STOS control laws derived in Section II applied to a model of a disk drive system are then given in Section III. Finally, concluding remarks are provided in Section IV.

II. Shaped Phase-Plane Control

A servomechanism consisting of a pure rigid body and multiple flexible modes can be modeled using a state space differential equation as follows:

$$\dot{\underline{\mathbf{x}}} = \mathbf{A}\underline{\mathbf{x}} + \mathbf{B}u \tag{1}$$

where

$$\mathbf{A} = \left[\begin{array}{cc|cccc} 0 & 1 & 0 & 0 & \cdots & 0 & 0 \\ 0 & 0 & 0 & 0 & \cdots & 0 & 0 \\ \hline 0 & 0 & 0 & 1 & \cdots & 0 & 0 \\ 0 & 0 & -\omega_{n1}^2 & -2\zeta_1\omega_{n1} & \cdots & 0 & 0 \\ \vdots & \vdots & \vdots & \vdots & \vdots & \vdots & \vdots \\ 0 & 0 & 0 & 0 & \cdots & 0 & 1 \\ 0 & 0 & 0 & 0 & \cdots & -\omega_{nM}^2 & -2\zeta_M\omega_{nM} \end{array}\right],$$

$$\mathbf{B} = \left[\begin{array}{cc|ccccc} 0 & b_2 & 0 & b_{41} & \cdots & 0 & b_{4M} \end{array}\right]',$$

$$\underline{\mathbf{x}} = \left[\begin{array}{cc|ccccc} x_r & \dot{x}_r & x_{f_1} & \dot{x}_{f_1} & \cdots & x_{f_M} & \dot{x}_{f_M} \end{array}\right]'.$$

The state $\underline{\mathbf{x}}$ represents positions, x_r and x_{fi}, and velocities, $\dot{x}_r$ and $\dot{x}_{fi}$, where rigid body and flexible body are denoted

This work was supported in part by the US National Science Foundation (Grant CMS-0201459) and the Colorado Center for Information Storage.

Chanat La-orpacharapan is a graduate student in the Electrical and Computer Engineering Department, University of Colorado, Boulder, CO 80309 *laorpach@colorado.edu.*

Lucy Pao is an associate professor in the Electrical and Computer Engineering Department, University of Colorado, Boulder, CO 80309 *pao@colorado.edu.*

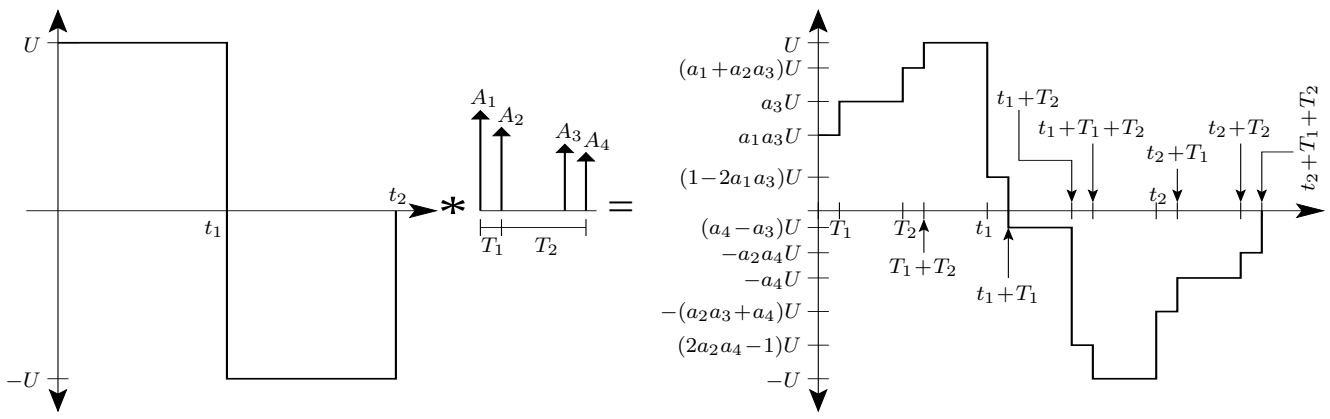

(a) Time-Optimal (b) Shaper (c) Shaped Time-Optimal

Fig. 1. Convolution of the bang-bang input with the four impulses of the convolution method shaper for two damped flexible modes yields the shaped bang-bang input, where $T_1 = \pi/\omega_{d1}$, $T_2 = \pi/\omega_{d2}$, $A_1 = a_1a_3$, $A_2 = a_2a_3$, $A_3 = a_1a_4$, and $A_4 = a_2a_4$.

by the subscripts r and f, respectively, and M is the number of the flexible modes. ω_{ni} is the natural frequency and ζ_i is the damping of the ith flexible mode.

For a maneuver in the "positive" direction ($X > 0$), the bang-bang input as shown in Fig. 1(a) that drives the rigid body portion of the system (1) from rest to rest in minimum time is

$$u(t) = \begin{cases} +U, & 0 \le t \le t_1 = \sqrt{\dfrac{|X|}{Ub_2}} \\ -U, & \sqrt{\dfrac{|X|}{Ub_2}} \le t \le t_2 = 2\sqrt{\dfrac{|X|}{Ub_2}} \end{cases}, \tag{2}$$

where U is the actuator limit and $|X|$ is the move distance. For maneuvers in the "negative" direction ($X < 0$), the signs of the two pulses are reversed, with the negative pulse first followed by the positive pulse.

For one flexible mode with natural frequency ω_n and damping ζ, the two impulses of the simplest zero vibration (ZV) shaper have the amplitudes of a_1 and a_2 and spacing of T which can be described as follows [13]:

$$T = \frac{\pi}{\omega_d}, \quad a_1 = \frac{1}{1+K}, \quad a_2 = \frac{K}{1+K}, \tag{3}$$

where

$$K = e^{-\frac{\zeta\pi}{\sqrt{1-\zeta^2}}},$$

and $\omega_d = \omega_n\sqrt{1-\zeta^2}$ is the damped natural frequency.

A. Convolution Method Shaper

An input shaper for multiple flexible modes can be obtained by designing the shaper from (3) for each flexible mode separately and then convolving the shapers together [12], [13]. For two flexible modes with damped frequencies ω_{d1} and ω_{d2}, the input shaper, as shown in Fig. 1(b), consists of four impulses occurring at times 0, $T_1 = \pi/\omega_{d1}$, $T_2 = \pi/\omega_{d2}$, and $T_2 + T_1 = \pi/\omega_{d1} + \pi/\omega_{d2}$, respectively. The amplitudes of the impulses are $A_1 = a_1a_3$, $A_2 = a_2a_3$, $A_3 = a_1a_4$, and $A_4 = a_2a_4$, where a_{2i-1} and a_{2i} are the amplitudes of the shaper for the ith flexible mode.

Using the input shaper as detailed above to shape the unshaped time-optimal input (2), we obtain the shaped time-optimal input, shown in Fig. 1(c), as follows:

$$u(t) = \begin{cases} a_1a_3U, & 0 \le t \le T_1 \\ a_3U, & T_1 \le t \le T_2 \\ (a_1+a_2a_3)U, & T_2 \le t \le T_1+T_2 \\ U, & T_1+T_2 \le t \le t_1 \\ (1-2a_1a_3)U, & t_1 \le t \le t_1+T_1 \\ (a_4-a_3)U, & t_1+T_1 \le t \le t_1+T_2 \\ (2a_2a_4-1)U, & t_1+T_2 \le t \le t_1+T_1+T_2 \\ -U, & t_1+T_1+T_2 \le t \le t_2 \\ -(a_2a_3+a_4)U, & t_2 \le t \le t_2+T_1 \\ -a_4U, & t_2+T_1 \le t \le t_2+T_2 \\ -a_2a_4U, & t_2+T_2 \le t \le t_2+T_1+T_2 \end{cases}. \tag{4}$$

The expression for this shaped input is derived assuming that $T_1 + T_2 = \pi/\omega_{d1} + \pi/\omega_{d2} < \sqrt{|X|/(Ub_2)}$ or $|X| > (\pi/\omega_{d1} + \pi/\omega_{d2})^2 Ub_2$ which holds for relatively high resonance frequencies or large maneuvers. In other words, the length of the shaper in this case is less than the length of each of the bang-bang pulses. Otherwise, the convolution of the impulses with the bang-bang input will lead to a different shaped profile. For different shaped profiles $\left(\text{such as when } \sqrt{|X|/(Ub_2)} < \pi/\omega_{d1}+\pi/\omega_{d2} < 2\sqrt{|X|/(Ub_2)} \text{ or when } \pi/\omega_{d1} + \pi/\omega_{d2} > 2\sqrt{|X|/(Ub_2)}\right)$, the STOS control law still can be derived using a similar procedure as detailed below for the particular shaped profile of (4). However, as discussed in [11], the STOS control laws for different shaped profiles might have to use a different phase-plane than the $(x_r, \dot{x}_r)$ phase-plane used in this paper.

Normally, the flexible modes in disk drive systems have relatively high frequencies (2 to 6 kHz) which leads to the shaper length being very small, and the assumption $|X| > (\pi/\omega_{d1} + \pi/\omega_{d2})^2 U b_2$ holds for the majority of maneuvers. Indeed, in disk drive systems, maneuver sizes such that $|X| < (\pi/\omega_{d1} + \pi/\omega_{d2})^2 U b_2$ are so small that they generally do not fall into the "seek" motion range, and a different type of controller (a "settling" controller) is usually used for this different mode of operation.

Applying the shaped input (4) into the system (1) yields the $(x_r, \dot{x}_r)$ phase-plane trajectories as shown in Fig. 2 for several maneuver sizes $|X|$. The states x_r and $\dot{x}_r$ at the switching times 0, T_1, T_2, T_1+T_2, t_1, t_1+T_1, t_1+T_2, $t_1+T_1+T_2$, t_2, t_2+T_1, t_2+T_2, and $t_2+T_1+T_2$ can be analytically determined as follows:

$$
\begin{aligned}
x_r = &-|X|, \quad -|X| + \frac{1}{2}a_1a_3Ub_2\left(\frac{\pi}{\omega_{d1}}\right)^2, \quad -|X| \\
&+ \frac{1}{2}a_2a_3Ub_2\left(\frac{\pi}{\omega_{d1}}\right)^2 - a_2a_3\frac{Ub_2\pi^2}{\omega_{d1}\omega_{d2}} + \frac{1}{2}a_3Ub_2\left(\frac{\pi}{\omega_{d2}}\right)^2, \\
&- |X| + \frac{1}{2}a_1Ub_2\left(\frac{\pi}{\omega_{d1}}\right)^2 + \frac{1}{2}a_3Ub_2\left(\frac{\pi}{\omega_{d2}}\right)^2 \\
&+ a_1a_3\frac{Ub_2\pi^2}{\omega_{d1}\omega_{d2}}, \quad -\frac{1}{2}|X| - \left(\frac{a_2\pi}{\omega_{d1}} + \frac{a_4\pi}{\omega_{d2}}\right)\sqrt{|X|Ub_2} \\
&+ a_2a_4\frac{Ub_2\pi^2}{\omega_{d1}\omega_{d2}} + \frac{1}{2}a_4Ub_2\left(\frac{\pi}{\omega_{d2}}\right)^2 + \frac{1}{2}a_2Ub_2\left(\frac{\pi}{\omega_{d1}}\right)^2, \\
&- \frac{1}{2}|X| + \frac{1}{2}a_1\left(a_4 - a_3\right)Ub_2\left(\frac{\pi}{\omega_{d1}}\right)^2 - a_1a_4\frac{Ub_2\pi^2}{\omega_{d1}\omega_{d2}} \\
&+ \frac{1}{2}a_4Ub_2\left(\frac{\pi}{\omega_{d2}}\right)^2 + \left(\frac{a_1\pi}{\omega_{d1}} - \frac{a_4\pi}{\omega_{d2}}\right)\sqrt{|X|Ub_2}, \\
&- \frac{1}{2}|X| + \frac{1}{2}a_2\left(a_4 - a_3\right)Ub_2\left(\frac{\pi}{\omega_{d1}}\right)^2 + a_2a_3\frac{Ub_2\pi^2}{\omega_{d1}\omega_{d2}} \\
&- \frac{1}{2}a_3Ub_2\left(\frac{\pi}{\omega_{d2}}\right)^2 - \left(\frac{a_2\pi}{\omega_{d1}} - \frac{a_3\pi}{\omega_{d2}}\right)\sqrt{|X|Ub_2}, \\
&- \frac{1}{2}|X| - \frac{1}{2}a_1Ub_2\left(\frac{\pi}{\omega_{d1}}\right)^2 - a_1a_3\frac{Ub_2\pi^2}{\omega_{d1}\omega_{d2}} \\
&- \frac{1}{2}a_3Ub_2\left(\frac{\pi}{\omega_{d2}}\right)^2 + \left(\frac{a_1\pi}{\omega_{d1}} + \frac{a_3\pi}{\omega_{d2}}\right)\sqrt{|X|Ub_2}, \\
&- \frac{1}{2}a_2Ub_2\left(\frac{\pi}{\omega_{d1}}\right)^2 - a_2a_4\frac{Ub_2\pi^2}{\omega_{d_1}\omega_{d2}} - \frac{1}{2}a_4Ub_2\left(\frac{\pi}{\omega_{d2}}\right)^2, \\
&- \frac{1}{2}a_1a_4Ub_2\left(\frac{\pi}{\omega_{d1}}\right)^2 + a_1a_4\frac{Ub_2\pi^2}{\omega_{d_1}\omega_{d2}} - \frac{1}{2}a_4Ub_2\left(\frac{\pi}{\omega_{d2}}\right)^2, \\
&- \frac{1}{2}a_2a_4Ub_2\left(\frac{\pi}{\omega_{d1}}\right)^2, \quad 0, \qquad (5)
\end{aligned}
$$

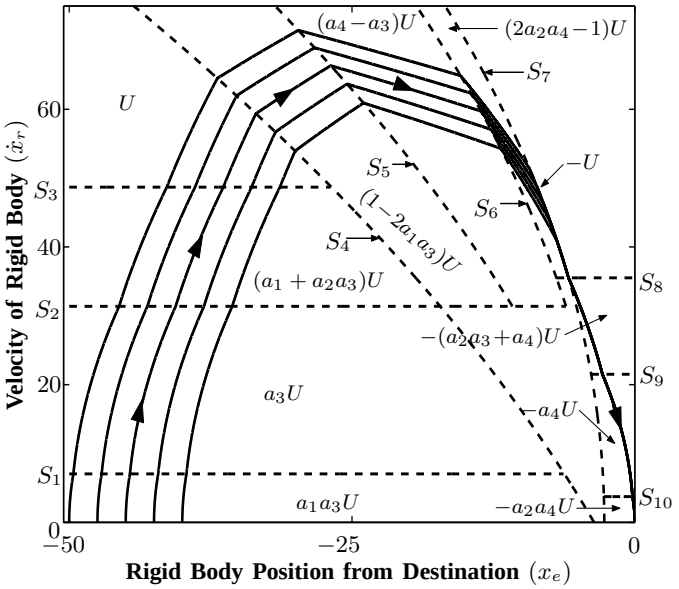

Fig. 2. Phase-plane trajectories (solid) and switching curves (dashed) resulting from the shaped time-optimal control derived from the convolution method shaper for two damped flexible modes.

$$
\begin{aligned}
&\dot{x}_r = 0, \quad a_1a_3Ub_2\frac{\pi}{\omega_{d1}}, \quad -a_2a_3Ub_2\frac{\pi}{\omega_{d1}} + a_3Ub_2\frac{\pi}{\omega_{d2}}, \\
&a_1Ub_2\frac{\pi}{\omega_{d1}} + a_3Ub_2\frac{\pi}{\omega_{d2}}, \quad -a_2Ub_2\frac{\pi}{\omega_{d1}} - a_4Ub_2\frac{\pi}{\omega_{d2}} \\
&+ \sqrt{|X|Ub_2}, \quad a_1\left(a_4 - a_3\right)Ub_2\frac{\pi}{\omega_{d1}} - a_4Ub_2\frac{\pi}{\omega_{d2}} \\
&+ \sqrt{|X|Ub_2}, \quad -a_2\left(a_4 - a_3\right)Ub_2\frac{\pi}{\omega_{d1}} - a_3Ub_2\frac{\pi}{\omega_{d2}} \\
&+ \sqrt{|X|Ub_2}, \quad -a_1Ub_2\frac{\pi}{\omega_{d1}} - a_3Ub_2\frac{\pi}{\omega_{d2}} + \sqrt{|X|Ub_2}\,, \\
&a_2Ub_2\frac{\pi}{\omega_{d1}} + a_4Ub_2\frac{\pi}{\omega_{d2}}, \quad -a_1a_4Ub_2\frac{\pi}{\omega_{d1}} + a_4Ub_2\frac{\pi}{\omega_{d2}}, \\
&a_2a_4Ub_2\frac{\pi}{\omega_{d1}}, \quad 0. \qquad (6)
\end{aligned}
$$

For maneuvers in the "positive" direction, the input has eleven different levels in (4) and therefore quadrant 2 of the phase-plane can be divided into eleven regions based on the shaped time-optimal input that should be applied to the plant.

In the first region, the input is a_1a_3U and switches to a_3U at the switching time T_1. From (6), the state $\dot{x}_r$ at the switching time T_1 is independent of the move distance $|X|$. Thus, the first switching curve is

$$S_1 = a_1a_3Ub_2\frac{\pi}{\omega_{d1}}. \qquad (7)$$

In the second through third and the ninth through eleventh regions, the inputs are a_3U, $(a_1+a_2a_3)U$, $-(a_2a_3+a_4)U$, $-a_4U$, and $-a_2a_4U$, respectively. Similarly, the duration of these shaped input pulses is independent of the move distance $|X|$ and is only a function of the natural frequencies ω_{d1} and ω_{d2}. Therefore the switching curves are the $\dot{x}_r$ states at the corresponding switching times and are as

follows:

$$S_2 = -a_2a_3Ub_2\frac{\pi}{\omega_{d1}} + a_3Ub_2\frac{\pi}{\omega_{d2}}, \quad (8)$$

$$S_3 = a_1Ub_2\frac{\pi}{\omega_{d1}} + a_3Ub_2\frac{\pi}{\omega_{d2}}, \quad (9)$$

$$S_8 = a_2Ub_2\frac{\pi}{\omega_{d1}} + a_4Ub_2\frac{\pi}{\omega_{d2}}, \quad (10)$$

$$S_9 = -a_1a_4Ub_2\frac{\pi}{\omega_{d1}} + a_4Ub_2\frac{\pi}{\omega_{d2}}, \quad (11)$$

$$S_{10} = a_2a_4Ub_2\frac{\pi}{\omega_{d1}}. \quad (12)$$

To solve for the fourth switching curve, we need to eliminate the move distance variable $|X|$ from the states x_r and $\dot{x}_r$ at the switching time t_1. After some algebraic manipulations, we obtain the fourth switching curve x_r in terms of $\dot{x}_r$ as follows:

$$\begin{aligned} S_4(\dot{x}_r) = &-\frac{1}{2Ub_2}\dot{x}_r^2 - 2\left(a_2\frac{\pi}{\omega_{d1}} + a_4\frac{\pi}{\omega_{d2}}\right)\dot{x}_r \\ &- 2a_2a_4Ub_2\frac{\pi^2}{\omega_{d1}\omega_{d2}} - \frac{1}{2}a_2\left(3a_2-1\right)Ub_2\left(\frac{\pi}{\omega_{d1}}\right)^2 \\ &- \frac{1}{2}a_4\left(3a_4-1\right)Ub_2\left(\frac{\pi}{\omega_{d2}}\right)^2. \end{aligned} \quad (13)$$

In a similar manner as solving for the fourth switching curve, we can obtain the switching curves S_5 through S_7 as follows:

$$\begin{aligned} S_5(\dot{x}_r) = &-\frac{1}{2Ub_2}\dot{x}_r^2 + 2a_4\left(a_1\frac{\pi}{\omega_{d1}} - \frac{\pi}{\omega_{d2}}\right)\dot{x}_r \\ &+ \frac{1}{2}a_1\left(a_4-a_3\right)\left(a_2-2a_1a_4\right)Ub_2\left(\frac{\pi}{\omega_{d1}}\right)^2 \\ &+ 2a_1a_4\left(a_4-a_3\right)Ub_2\frac{\pi^2}{\omega_{d1}\omega_{d2}} \\ &+ \frac{1}{2}a_4\left(1-3a_4\right)Ub_2\left(\frac{\pi}{\omega_{d2}}\right)^2, \end{aligned} \quad (14)$$

$$\begin{aligned} S_6(\dot{x}_r) = &-\frac{1}{2Ub_2}\dot{x}_r^2 - 2a_2a_4\frac{\pi}{\omega_{d1}}\dot{x}_r - \frac{1}{2}a_3a_4Ub_2\left(\frac{\pi}{\omega_{d2}}\right)^2 \\ &+ \frac{1}{2}a_2\left(a_4-a_3\right)\left(a_1-2a_2a_4\right)Ub_2\left(\frac{\pi}{\omega_{d1}}\right)^2, \end{aligned} \quad (15)$$

$$\begin{aligned} S_7(\dot{x}_r) = &-\frac{1}{2Ub_2}\dot{x}_r^2 - \frac{1}{2}a_1a_2Ub_2\left(\frac{\pi}{\omega_{d1}}\right)^2 \\ &- \frac{1}{2}a_3a_4Ub_2\left(\frac{\pi}{\omega_{d2}}\right)^2. \end{aligned} \quad (16)$$

Ideally, the trajectory does not go beyond the switching curve S_7. However, in practice, overshoot will likely occur due to discrete sampling times or other implementation issues. Thus, we assign the input $-U$ for the region to the right of the switching curve S_7.

The switching curves for the fourth quadrant (for maneuvers in the "negative" direction) can be derived similarly as done above for the second quadrant. In fact, the switching curves for the fourth quadrant are anti-symmetric to the switching curves for the second quadrant.

For rest-to-rest motions, the first and third quadrants ideally are never entered. However, in practice, disturbances or non-ideal behavior may cause the state of the system to move into either the first or third quadrant. Hence, control values of $-U$ and $+U$ are assigned to the first and third quadrants, respectively, so that the system will be caused to move into the second or fourth quadrant as quickly as possible, and the goal is that the control action in the second and fourth quadrants brings the system to the origin in the respective quadrant.

The STOS closed-loop control law for all four quadrants for systems with two damped flexible modes derived by using the convolution method shaper can be expressed as a logic expression as follows:

$$\begin{aligned} u = &-U\,\mathrm{sgn}\left(x_e\right)\mathrm{sgn}\left(\dot{x}_r\right)\left[\frac{\mathrm{sgn}\left(x_e\right)+1}{2}\right]\left[\frac{\mathrm{sgn}\left(\dot{x}_r\right)+1}{2}\right] \\ &+ U\,\mathrm{sgn}\left(-\dot{x}_r\right)\Big[1-\mathrm{sgn}\left(|x_e|\right)\Big] + U\,\mathrm{sgn}\left(-x_e\right)\mathrm{sgn}\left(-\dot{x}_r\right) \\ &\times\left[\frac{\mathrm{sgn}\left(-x_e\right)+1}{2}\right]\left[\frac{\mathrm{sgn}\left(-\dot{x}_r\right)+1}{2}\right] + f_1\left(\cdot\right)\mathrm{sgn}\left(-x_e\right) \\ &\times\left[\frac{\mathrm{sgn}\left(-x_e\right)+1}{2}\right]\Bigg\{\mathrm{sgn}\left(\dot{x}_r\right)\left[\frac{\mathrm{sgn}\left(\dot{x}_r\right)+1}{2}\right] \\ &+ 1 - \mathrm{sgn}\left(|\dot{x}_r|\right)\Bigg\} + f_2\left(\cdot\right)\mathrm{sgn}\left(x_e\right)\left[\frac{\mathrm{sgn}\left(x_e\right)+1}{2}\right] \\ &\times\left\{\mathrm{sgn}\left(-\dot{x}_r\right)\left[\frac{\mathrm{sgn}\left(-\dot{x}_r\right)+1}{2}\right] + 1 - \mathrm{sgn}\left(|\dot{x}_r|\right)\right\}, \end{aligned} \quad (17)$$

where

$$\begin{aligned} f_1(\cdot) = &\ UD\,\mathrm{sgn}(D+1)\Big\{\mathrm{sgn}(C+1) + H\,\mathrm{sgn}(H+1) \\ &\times\Big[\left(a_1+a_2a_3\right)C\,\mathrm{sgn}(B+1)\mathrm{sgn}(C-1) + a_3B \\ &\times\mathrm{sgn}(A+1)\mathrm{sgn}(B-1) + a_1a_3A\,\mathrm{sgn}(A-1)\Big]\Big\} \\ &- UQ\,\mathrm{sgn}(Q+1)\Big[-\mathrm{sgn}(H-1) + \left(a_4-a_3\right)GH \\ &\times\mathrm{sgn}(E-1)\mathrm{sgn}(G+1)\mathrm{sgn}(H+1) + (2a_2a_4-1) \\ &\times H\mathrm{sgn}(G-1)\mathrm{sgn}(H+1)\Big] - (1-2a_1a_3)\,UBEH \\ &\times\mathrm{sgn}(B+1)\mathrm{sgn}(D-1)\mathrm{sgn}(E+1)\mathrm{sgn}(H+1) \\ &+ UH\,\mathrm{sgn}(H-1)\Big[\left(a_2a_3+a_4\right)R\,\mathrm{sgn}(Q-1) \\ &\times\mathrm{sgn}(R+1) + a_4S\mathrm{sgn}(R-1)\mathrm{sgn}(S+1) \\ &+ a_2a_3\,\mathrm{sgn}(S-1)\Big], \end{aligned} \quad (18)$$

and

$$\begin{aligned} A = \mathrm{sgn}(\dot{x}_r - S_1), &\quad B = \mathrm{sgn}(\dot{x}_r - S_2), \\ C = \mathrm{sgn}(\dot{x}_r - S_3), &\quad Q = \mathrm{sgn}(\dot{x}_r - S_8), \\ R = \mathrm{sgn}(\dot{x}_r - S_9), &\quad S = \mathrm{sgn}(\dot{x}_r - S_{10}), \end{aligned}$$

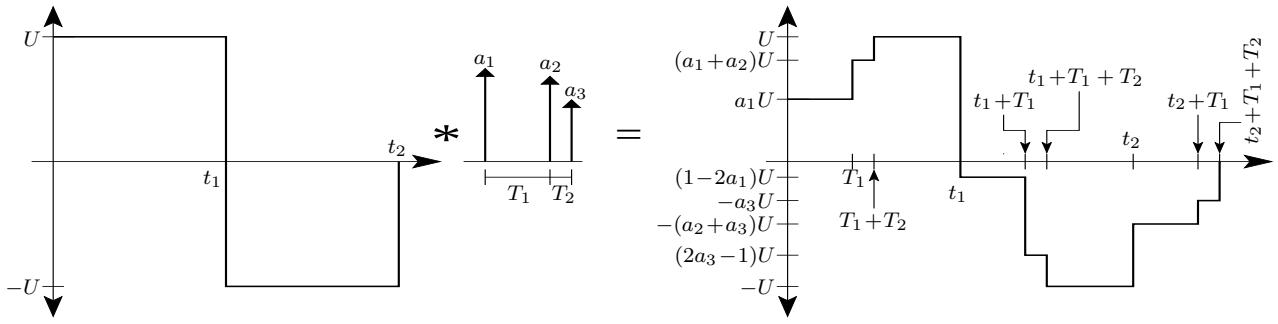

(a) Time-Optimal (b) Shaper (c) Shaped Time-Optimal

Fig. 3. Convolution of the bang-bang input with three impulses of the simultaneous method shaper for two damped flexible modes yields the shaped bang-bang input.

$$D = \text{sgn}(S_4(\dot{x}_r) - x_e), \quad E = \text{sgn}(S_5(\dot{x}_r) - x_e),$$
$$G = \text{sgn}(S_6(\dot{x}_r) - x_e), \quad H = \text{sgn}(S_7(\dot{x}_r) - x_e),$$

and $x_e = x_r - |X|$ is the distance of the rigid body position from the destination and the switching curves S_1 through S_{10} are described in (7) - (9), (13) - (16), and (10) - (12), respectively. The factor $1 - \text{sgn}(|x_e|)$ determines whether the state of the system is on the $\dot{x}_r$ axis of the phase-plane. Similarly, the term $1 - \text{sgn}(|\dot{x}_r|)$ determines if the state is on the x_e axis. $f_1(\cdot)$ is the switching function for the second quadrant and $f_2(\cdot)$ is the switching function for the fourth quadrant which can be described as

$$f_2(x_e, \dot{x}_r) = -f_1(-x_e, -\dot{x}_r). \tag{19}$$

B. Simultaneous Method Shaper

In some applications, it is preferable to have a smaller number of times that the command input changes its value. For M flexible modes, instead of solving for the input shaper with the convolution method, we can reduce the number of the impulses of the multi-mode input shaper from 2^M to $M+1$ by solving for the input shaper with the "simultaneous" method.

Input shapers for M multiple flexible modes can be derived by directly solving the impulse amplitudes a_i and times t_i from the following $2M+1$ constraint equations [12], [13]:

$$\begin{aligned}
\sum_{i=1}^{N} a_i e^{-\zeta_j \omega_{n_j}(t_N - t_i)} \sin\left(\omega_{n_j} t_i \sqrt{1-\zeta_j^2}\right) &= 0, \\
\sum_{i=1}^{N} a_i e^{-\zeta_j \omega_{n_j}(t_N - t_i)} \cos\left(\omega_{n_j} t_i \sqrt{1-\zeta_j^2}\right) &= 0, \\
\sum_{i=1}^{N} a_i &= 1,
\end{aligned} \tag{20}$$

for $j = 1, 2, ..., M$.

The simultaneous method shaper for two flexible modes consists of three impulses with spacings T_1 and T_2 and the amplitudes of a_1, a_2, and a_3 as shown in Fig. 3(b). Assuming that each pulse width of the time-optimal input (2) is longer than the shaper length $T_1 + T_2$ then the shaped time-optimal input, as illustrated in Fig. 3(c), is as follows:

$$u(t) = \begin{cases}
a_1 U, & 0 \le t \le T_1 \\
(a_1 + a_2)U, & T_1 \le t \le T_1 + T_2 \\
U, & T_1 + T_2 \le t \le t_1 \\
(1 - 2a_1)U, & t_1 \le t \le t_1 + T_1 \\
(2a_3 - 1)U, & t_1 + T_1 \le t \le t_1 + T_1 + T_2 \\
-U, & t_1 + T_1 + T_2 \le t \le t_2 \\
-(a_2 + a_3)U, & t_2 \le t \le t_2 + T_1 \\
-a_3 U, & t_2 + T_1 \le t \le t_2 + T_1 + T_2
\end{cases}. \tag{21}$$

Through a similar procedure as solving for the STOS control law using the convolution method shaper, the STOS control law for two damped flexible mode systems resulting from the simultaneous method shaper is as in (17) and (19), where $f_1(\cdot)$ is

$$\begin{aligned}
f_1(\cdot) = {} & UC\,\text{sgn}(C+1)\Big[(a_2+a_3)\,AE\,\text{sgn}(A-1) \\
& \times \text{sgn}(E+1) + (a_1+a_2)\,BE\,\text{sgn}(A+1)\text{sgn}(B-1) \\
& \times \text{sgn}(E+1) + \text{sgn}(B+1)\Big] + UG\,\text{sgn}(G+1) \\
& \times \Big[(2a_1-1)\,DE\,\text{sgn}(C-1)\text{sgn}(D+1)\text{sgn}(E+1) \\
& + (1-2a_3)\,E\,\text{sgn}(D-1)\text{sgn}(E+1) + \text{sgn}(E-1)\Big] \\
& + UE\,\text{sgn}(E-1)\Big[(a_2+a_3)\,H\,\text{sgn}(G-1)\text{sgn}(H+1) \\
& + a_3\,\text{sgn}(H-1)\Big],
\end{aligned} \tag{22}$$

where

$$\begin{aligned}
A &= \text{sgn}(\dot{x}_r - S_1), & B &= \text{sgn}(\dot{x}_r - S_2), \\
G &= \text{sgn}(\dot{x}_r - S_6), & H &= \text{sgn}(\dot{x}_r - S_7), \\
C &= \text{sgn}(S_3(\dot{x}_r) - x_e), & D &= \text{sgn}(S_4(\dot{x}_r) - x_e), \\
E &= \text{sgn}(S_5(\dot{x}_r) - x_e),
\end{aligned}$$

and the switching curves S_1 through S_7, as shown in Fig. 4,

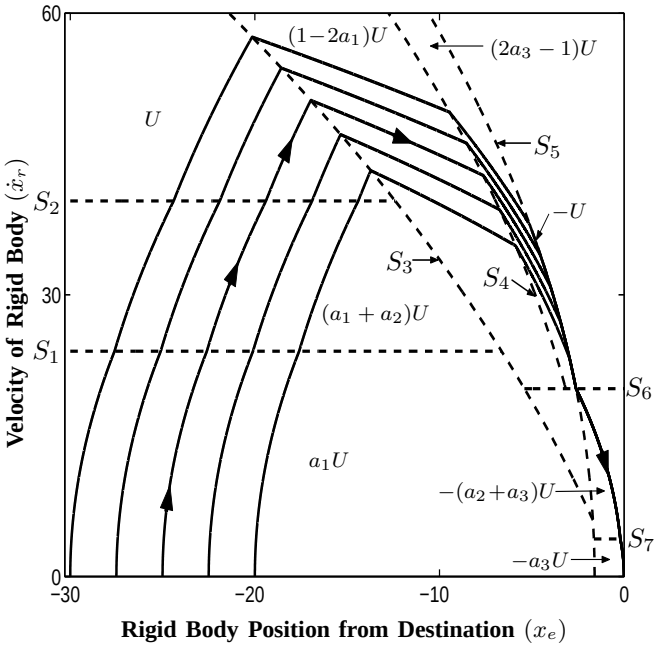

Fig. 4. Phase-plane trajectories (solid) and switching curves (dashed) due to the shaped time-optimal control derived by the simultaneous shaper for two damped flexible modes.

are as follows:

$$S_1 = a_1 U b_2 T_1,$$

$$S_2 = a_1 U b_2 T_1 + (a_1 + a_2)\, U b_2 T_2,$$

$$S_3(\dot{x}_r) = -\frac{1}{2Ub_2}\dot{x}_r + 2\Big[(a_1 - 1)\, T_1 - a_3 T_2\Big]\dot{x}_r + \frac{1}{2}(a_1 - 1)(2 - 3a_1)\, U b_2 T_1^2 + \frac{1}{2}a_3 (1 - 3a_3)\, U b_2 T_2^2 + a_3 (3a_1 - 2)\, U b_2 T_1 T_2,$$

$$S_4(\dot{x}_r) = -\frac{1}{2Ub_2}\dot{x}_r^2 - 2a_3 T_2 \dot{x}_r + \frac{1}{2}a_1 (a_1 - 1)\, U b_2 T_1^2 + \frac{1}{2}a_3 (1 - 3a_3)\, U b_2 T_2^2 - a_1 a_3 U b_2 T_1 T_2,$$

$$S_5(\dot{x}_r) = -\frac{1}{2Ub_2}\dot{x}_r^2 + \frac{1}{2}a_1 (a_1 - 1)\, U b_2 T_1^2 - \frac{1}{2}a_3 (a_1 + a_2)\, U b_2 T_2^2 - a_1 a_3 U b_2 T_1 T_2,$$

$$S_6 = (1 - a_1)\, U b_2 T_1 + a_3 U b_2 T_2,$$

$$S_7 = a_3 U b_2 T_2.$$

III. Simulation Results and Discussion

The derived STOS control is a feedback control law which automatically handles some set point changes without having to re-compute the shaped feedforward command. The length of the STOS control is longer than the time-optimal control by at most the length of the input shaper. For systems having M modes, the length of the convolution method shaper is equal to $\sum_{i=1}^{M} \pi/\omega_{di}$ which is longer than the length of the simultaneous shaper. While the STOS control is slightly longer than the time-optimal control, solving for the time-optimal control for the sixth- or higher-order system is very difficult.

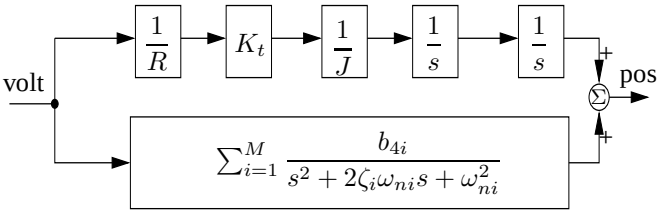

Fig. 5. Block diagram of a structure with M flexible modes driven by a voice coil motor. R, K_t, and J are coil resistance, torque constant, and motor inertia, respectively.

Fig. 6 shows the responses of the STOS control laws for two damped flexible modes derived using the convolution and simultaneous method shapers. A model of a disk drive system as shown in Fig. 5 with parameter values given in Table I is used. The flexible modes have frequencies and damping ratios of $f_{n1} = 2.0 \times 10^3$ Hz, $\zeta_1 = 0.01$, $f_{n2} = 3.0 \times 10^3$ Hz, and $\zeta_2 = 0.01$. The input shaper derived using the convolution method for these two flexible modes has four impulses with the amplitudes of $A_1 = a_1 a_3 = 0.2579$, $A_2 = a_2 a_3 = 0.2499$, $A_3 = a_1 a_4 = 0.2499$, and $A_4 = a_2 a_4 = 0.2422$ and occur at times 0 s, 1.6668×10^{-4} s, 2.5001×10^{-4} s, and 4.1669×10^{-4} s. The input shaper derived from the simultaneous method for these two damped flexible modes has three impulses with the amplitudes of $a_1 = 0.2848$, $a_2 = 0.4471$, and $a_3 = 0.2681$ and occur at times 0 s, 2.0135×10^{-4} s, and 4.0461×10^{-4} s, respectively. Fig. 6 shows that the derived STOS control laws lead to rest-to-rest motion without unwanted residual vibration.

It can be seen that the length of the simultaneous method shaper is shorter than the convolution method shaper, leading to the STOS control derived from the simultaneous method shaper being shorter than that derived from the convolution method shaper by 1.208×10^{-5} s or 2.9%. However, the STOS control derived using the simultaneous method shaper, as described in (22), consists of the amplitude and spacing variables of the impulses of the shaper a_1, a_2, a_3, T_1, T_2, and T_3 that need to be computed for the flexible system. Solving for the amplitudes and spacings of the impulses of the simultaneous method shaper from the non-linear constraint equations in (20) requires a complex numerical method [12] while convolution method shapers are easily determined analytically.

For systems having three or more flexible modes, the STOS control law can be derived using a similar procedure as detailed in Section II [7]. The trade-off between the STOS control derived using the simultaneous method shaper over the convolution method shaper is that the STOS control law derived using the simultaneous method shaper has shorter maneuver times and fewer switching times, but it requires complex numerical computations to solve the non-linear constraint equations (20) for the input shaper.

The computation of the convolution method shaper for multiple flexible modes is simple and has a closed-form

TABLE I

VOICE COIL MOTOR AND FLEXIBLE STRUCTURE PARAMETER VALUES. FOR THESE PARAMETER VALUES IN THE STATE-SPACE MODEL OF (1), $b_2 = -b_{4i} = 2.7 \times 10^3$ /(V s^2).

Parameter	Disk Drive Value
K_t	9.8×10^{-2} N · m/A
R	7.25 Ω
J	5×10^{-6} kg · m · m
U	11 V

solution. However, the number of impulses in an M-mode convolution input shaper is 2^M which leads to the STOS control having $3 \times 2^M - 1$ levels. Hence, the STOS control law derived using the convolution method shaper is practical for applications that have only a few unwanted dominant flexible modes.

Future work will include deriving a STOS control with a finite switching slope as well as transitioning the STOS control to a linear control when state trajectories approach the destination to further improve performance in the presence of modeling errors, disturbances, and discrete sampling times.

IV. CONCLUSIONS

Shaped time-optimal closed-loop control laws using a phase-plane approach for systems with two flexible modes have been derived. Both convolution and simultaneous method shapers are used to shape the time-optimal phase-plane trajectories of the rigid body portion of the system to address the flexible dynamics. The shaped time-optimal control laws derived by using the simultaneous method shaper yield faster time responses and fewer switches than using the convolution method shaper. However, numerical methods are required for solving simultaneous method shapers.

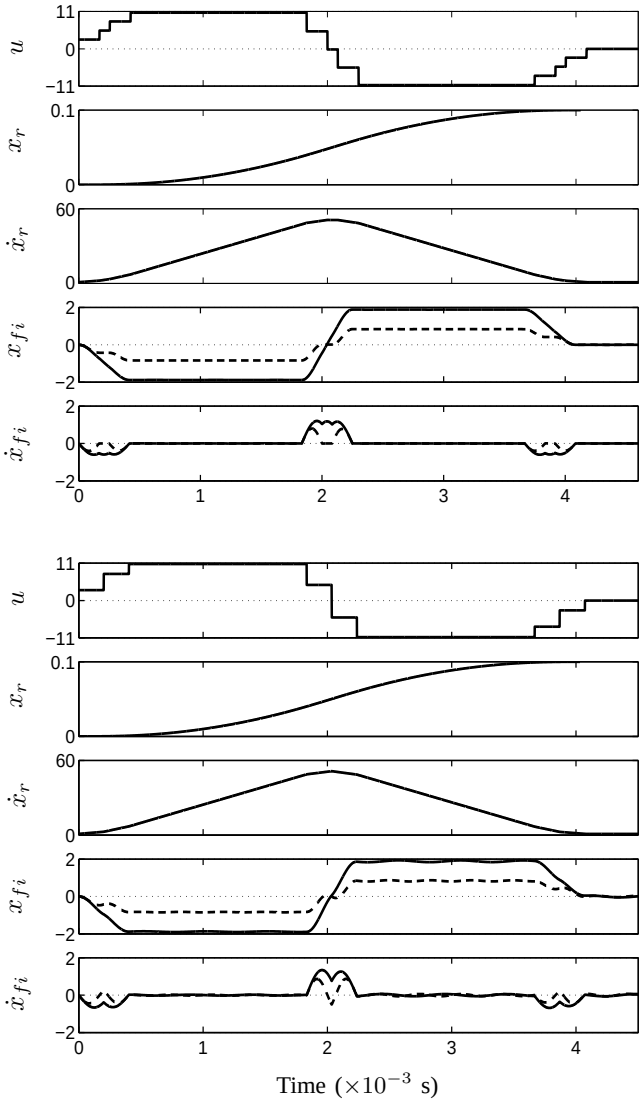

Fig. 6. Time response of the STOS control law derived from the convolution shaper (top) and the simultaneous shaper (bottom) for a system having two flexible modes: $f_{n1} = 2.0 \times 10^3$ Hz (solid) and $f_{n2} = 3.0 \times 10^3$ Hz (dashed). u, x_r, $\dot{x}_r$, x_{fi}, and $\dot{x}_{fi}$ are measured in volt, rad, rad/s, $\times 10^{-4}$ rad, and rad/s, respectively.

REFERENCES

[1] W. J. Book. "Controlled Motion in an Elastic World," *ASME J. Dyn. Sys., Meas., and Ctrl.*, 115(2), June 1993.

[2] G. F. Franklin, J. D. Powell, and M. L. Workman. *Digital Control of Dynamic Systems*, Reading, MA: Addison-Wesley, 1998.

[3] J. L. Junkins and Y. Kim. *Introduction to Dynamics and Control of Flexible Structures*, American Institute of Aeronautics and Astronautics, Washington, D.C., 1993.

[4] C. La-orpacharapan and L. Y. Pao. "Shaped Time-Optimal Feedback Control for Disk Drive Systems with Back-Electromotive Force," *IEEE Trans. Magnetics*, 40(1), Jan. 2004.

[5] C. La-orpacharapan and L. Y. Pao. "Shaped Phase-Plane Control for Disk Drive Systems with Back EMF, Slew Rate Limits, and Different Acceleration and Deceleration Rates," *Proc. Amer. Ctrl. Conf.*, June 2003.

[6] C. La-orpacharapan and L. Y. Pao. "Fast Seek Control for Flexible Disk Drive Systems with Back EMF and Inductance," *Proc. Amer. Ctrl. Conf.*, June 2003.

[7] C. La-orpacharapan. "Shaped Time-Optimal Closed-Loop Servomechanisms," University of Colorado, Ph.D. Thesis, Feb. 2004.

[8] W. S. Newman. "Robust Near Time-Optimal Control," *IEEE Trans. Aut. Ctrl.*, 35(7), July 1990.

[9] L. Y. Pao and G. F. Franklin. "Proximate Time-Optimal Control of Third-Order Servomechanisms," *IEEE Trans. Aut. Ctrl.*, 38(4), April 1993.

[10] L. Y. Pao and G. F. Franklin. "The Robustness of a Proximate Time-Optimal Controller," *IEEE Trans. Aut. Ctrl.*, 39(9), Sept. 1994.

[11] L. Y. Pao and C. La-orpacharapan. "Shaped Time-Optimal Feedback Controllers for Flexible Structures," *ASME J. Dyn. Sys., Meas., and Ctrl.*, 126(1), Mar. 2004.

[12] B. W. Rappole, N. C. Singer, and W. P. Seering. "Multiple-Mode Input Shaping Sequences for Reducing Residual Vibrations," *ASME Mechanisms Conf.*, 1994.

[13] N. C. Singer and W. P. Seering. "Preshaping Command Inputs to Reduce System Vibration," *ASME J. Dyn. Sys., Meas., and Ctrl.*, 112(1), Mar. 1990.

[14] T. D. Tuttle and W. P. Seering. "A Zero-Placement Technique for Designing Shaped Inputs to Suppress Multiple-Mode Vibration," *Proc. Amer. Ctrl. Conf.*, 1994.

[15] M. L. Workman and G. F. Franklin. "Implementation of Adaptive Proximate Time-Optimal Controllers," *Proc. Amer. Ctrl. Conf.*, June 1988.